Journal of Applied Analysis and Computation
Volume 16, Number 6, December 2026, 3264–3278
Website:http://www.jaac-online.com
DOI:10.11948/20250276

HIGH-ORDER ISOGEOMETRIC ANALYSIS FOR STOKES PROBLEM WITH NON-CONSTANT VISCOSITY

Lahcen El Ouadefli[1,†], Abdeslam El Akkad[1,2] and Ahmed Elkhalfi[1]

Abstract This paper investigates a high-order mixed isogeometric analysis for the Stokes problem with variable viscosity. We proposed and analyzed a new numerical scheme that can be viewed as a generalization of the classical Taylor–Hood elements. The numerical experiments are provided to validate the efficiency of scheme proposed.

Keywords Isogeometric analysis, inf-sup condition, error estimate, Stokes problem.

MSC(2010) 65N30, 65N15, 65G99, 76D07, 76D99.

1. Introduction

Isogeometric Analysis (IGA) has emerged as a powerful numerical methodology for the approximation of partial differential equations (PDEs), bridging the gap between Computer-Aided Design (CAD) and numerical simulation. Originally introduced by Hughes, Cottrell, and Bazilevs [18], IGA relies on spline-based functions, such as B-splines and NURBS, which allow an exact representation of complex geometries while simultaneously providing a highly regular approximation space.

The incompressible Stokes equations, wherein the viscosity of the fluid is contingent upon its spatial distribution, represent a critical framework in numerous scientific investigations, notably in simulations of phenomena such as the convective mantle dynamics. In these scenarios, the viscosity of the fluid can vary significantly across different regions, spanning several orders of magnitude. This variability poses a substantial challenge in accurately capturing the intricate behavior of the system. For instance, in studies of mantle convection, where the movement of Earth's rocky shell plays a crucial role in geological processes, understanding the intricate interplay between temperature, pressure, and viscosity gradients is paramount. Numerical simulations employing the incompressible Stokes equations with spatially varying viscosity provide a means to delve into these complexities and unravel the underlying mechanisms governing mantle dynamics. By accounting for the nuanced variations in viscosity, researchers can elucidate phenomena such as plate tectonics, magma migration, and seismic activity, contributing to advancements in our understanding of Earth's evolution and geophysical processes. This approach,

[†]The corresponding author.
[1]The Science and Engineering Research Laboratory, Faculty of Sciences and Techniques, Sidi Mohammed Ben Abdellah University, B.P. 2202 Route Imouzzer, Fes 30000, Morocco
[2]Departement de Mathématiques, Centre Régional des Métiers d'Éducation et de Formation de Fès-Meknès (CRMEF Fès-Meknès), Rue de Koweit 49, Ville Nouvelle, Fes 30050, Morocco
Email: lahcen.elouadefli@usmba.ac.ma(L. El ouadefli),
abdeslam.elakkad@usmba.ac.ma(A. El akkad), ahmed.elkhalfi@usmba.ac.ma(A. Elkhalfi)

detailed extensively in literature [11, 19, 22]. While numerous numerical schemes exist for solving the Stokes equations, many of them are primarily focused on scenarios where fluid viscosity remains constant [1, 12, 16, 19, 32]. However, in real-world applications such as geophysics and biomechanics [24, 28, 29], where viscosity can vary significantly across space, these conventional approaches may fall short in capturing the intricate dynamics accurately.

In such cases, the utilization of mixed finite element methods based on Non-Uniform Rational B-Splines (NURBS) emerges as a powerful alternative [3,6–8,10,14,15,18,23,25,27,31]. NURBS-based methods offer several advantages, notably their ability to represent complex geometries and adaptively refine the mesh, thereby enhancing the accuracy and efficiency of simulations. Moreover, NURBS provide a flexible framework for incorporating spatially varying viscosity, allowing researchers to tackle problems involving non-uniform fluid properties with greater fidelity.

The development of the mixed finite element method traditional in the context of Stokes problems with variable viscosity is introduced in [20, 26], the aim of this research is to expand upon existing numerical analysis and experimental studies by incorporating a stabilized Isogeometric Analysis (IGA) scheme, utilizing the Taylor-Hood element [2], to tackle the complexities of the Stokes equation with non-constant viscosity. By integrating IGA with the Taylor-Hood element, this study seeks to enhance the accuracy and stability of numerical simulations, particularly in scenarios where viscosity varies across the fluid domain.

The structure of this paper is organized as follows: Section 2 introduces the preliminary concepts related to NURBS functions. In Section 3, we present the model problem along with its weak formulation. Section 4 is devoted to the description of our numerical scheme and the details of the algebraic formulation of the problem. Finally, Section 5 is dedicated to the presentation of numerical results and the discussion of the convergence behavior.

2. The B-spline and NURBS preliminary

For a given knots set $\mathcal{E} = \{\xi_1 = 0, \ldots, \xi_i, \ldots, \xi_{n+p+1} = 1\}$, the B-spline function can be defined by the Cox-de Boor approach (see [5]) as the following

For $p = 0$:

$$N_i^0(\xi) = \begin{cases} 1 & \text{if} \quad \xi_i \leqslant \xi < \xi_{i+1}, \\ 0 & \text{otherwise}, \end{cases} \tag{2.1}$$

and, for $p \geqslant 1$:

$$\mathrm{N}_{\mathrm{i}}^{\mathrm{p}}(\xi) = \frac{\xi - \xi_{\mathrm{i}}}{\xi_{\mathrm{i+p}} - \xi_{\mathrm{i}}} \mathrm{N}_{\mathrm{i}}^{\mathrm{p}-1}(\xi) + \frac{\xi_{\mathrm{i+p+1}} - \xi}{\xi_{\mathrm{i+p+1}} - \xi_{\mathrm{i+1}}}\, \mathrm{N}_{\mathrm{i+1}}^{\mathrm{p}-1}(\xi). \tag{2.2}$$

A spline curve with order p in one dimension is defined as a linear combination of B-spline basis and control points $\mathbf{P}_i$

$$C(\xi) = \sum_{i=1}^{n} \mathrm{N}_i^p(\xi)\mathbf{P}_i, \tag{2.3}$$

From the knots vector $\mathcal{E}$, the break knots vector can builds as

$$\Xi = \{\zeta_1 = 0, \ldots, \zeta_i, \ldots, \zeta_m = 1\}, \tag{2.4}$$

where $\zeta_1 \prec \ldots \prec \zeta_i \prec \ldots \prec \zeta_m$, B-spline globally $\alpha_i = p - r_{\mathrm{i}}$-continuously differentiable at each knot ζ_i, where the sequence vector $\{r_1, \ldots, r_i, \ldots, r_m\}$, presented the multiplicities of the knots vector Ξ. On the case $r_1 = r_m = p + 1$, Ξ is called open knot.

Then, on $\widehat{\Omega} = [0, 1]$ parametric domain, the space generated from the univariate B-spline in 1-dimension is defined as follows

$$\hat{\mathcal{N}}_{\alpha}^{p} := \operatorname{span}\{N_i^p\}_{i=1}^n . \tag{2.5}$$

In the same way, by using the tensor product of two basis N_i^p and N_j^q associated with two break knots vector $\eta_1 = \{\zeta_{1,1} = 0, \ldots, \zeta_{1,i}, \ldots, \zeta_{1,n+p+1} = 1\}$ and $\eta_2 = \{\zeta_{2,1} = 0, \ldots, \zeta_{2,j}, \ldots, \zeta_{2,m+q+1} = 1\}$, respectively.

The 2-dimensional spline space on $\widehat{\Omega} = [0, 1] \times [0, 1]$ can be written

$$\hat{\mathcal{N}}_{\alpha}^{\mathbf{p}} := \operatorname{span}\left\{N_{i,j}^{p,q}\right\}_{i,j=1}^{m,n}, \tag{2.6}$$

here $\mathbf{p} = (p, q)$ and $\alpha = (\alpha_1, \alpha_2)$.

Starting from B-spline functions, univariate NURBS functions are defined as follows

$$R_i^p(\xi) = \frac{N_i{}^p(\xi) w_i}{\sum_{j=1}^n N_j^p(\xi) w_j}. \tag{2.7}$$

Here, w_i represents the weight assigned to the i-th control point, and it must be nonnegative.

A Non-Uniform Rational B-Spline (NURBS) curve with order p on 2D, denoted as

$$\hat{\mathrm{C}}(\xi) = \sum_{\mathrm{i}=1}^{\mathrm{n}} \mathrm{R}_{\mathrm{i}}^{\mathrm{p}}(\xi) \mathbf{P}_{\mathrm{i}}, \tag{2.8}$$

where $\mathbf{P}_i$ control points.

In the $\widehat{\Omega} = [0, 1]$, the univariate NURBS space generated from the NURBS basis R_i^p is referred via:

$$\hat{\mathcal{N}}_{\alpha}^{p} := \operatorname{span}\{R_i^p\}_{i=1}^n . \tag{2.9}$$

In the same way as B-spline, In the parametric domain $\widehat{\Omega} = [0, 1] \times [0, 1]$, the multivariate NURBS space defined as

$$\hat{\mathcal{N}}_{\alpha_1,\alpha_2}^{p,q} := \operatorname{span}\left\{R_{i,j}^{p,q}\right\}_{i,j=1}^{n,m}, \tag{2.10}$$

where $R_{i,j}^{p,q} = \frac{N_i^p(\xi) M_j^q(\eta) w_{i,j}}{\sum_l^n \sum_k^m N_l^p(\xi) M_k^q(\eta) w_{l,k}}$.

The geometric NURBS mappping $\mathbf{F} : \widehat{\Omega} \to \Omega$ is then defined by:

$$\mathbf{F} = \sum_{\mathrm{i,j}=1}^{\mathrm{n,m}} \mathrm{R}_{\mathrm{i,j}}^{\mathrm{p,q}}(\xi) \mathbf{P}_{\mathrm{i,j}}, \tag{2.11}$$

where $\mathbf{P}_{\mathrm{i,j}}$ are referred as control points.

The mesh $(\mathcal{T}_h)_h$ associate with the break knot vectors η_1 and η_2 is a partition of $[0, 1] \times [0, 1]$ into rectangles

$$T_h := \{T = (\xi_{1,i}, \xi_{1,i+1}) \otimes (\xi_{2,j}, \xi_{2,j+1}), i = 1, \ldots, n-1; j = 1, \ldots, m-1\}. \tag{2.12}$$

The parameter h, representing the global mesh size, is given by:

$$h := \max\{h_T = \operatorname{Diam}(T), \quad T \in T_h\}, \tag{2.13}$$

the family of mesh $(\mathrm{T}_h)_h$ on the physical domain, naturally generated by $\mathbf{F}$ such as

$$K_h = \{K : \mathrm{K} = \mathbf{F}(T), T \in T_h\}, \tag{2.14}$$

where T is the pre-image of K by the mapping $\mathbf{F}$, the global mesh size is proven by

$$h = \max\{h_K, K \in K_h\}, \tag{2.15}$$

with $h_K = \|D\mathbf{F}\|_{L^\infty(Q)} h_K$.

The NURBS space over Ω is defined as the push-forward of the NURBS space $\hat{\mathcal{N}}$ on the parametric domain $\widehat{\Omega}$ i.e.

$$\mathcal{R}^{p,q}_{\alpha_1,\alpha_2} := \operatorname{span}\left\{R^{p,q}_{i,j} \circ \mathbf{F}^{-1} \mid i = 1,\dots,n-1; j = 1,\dots,m-1\right\}. \tag{2.16}$$

3. Model problem and weak form

Let Ω be an open domain of $\mathbb{R}^2$ with Lipchitz boundary Γ, for a steady flow ($\partial_t u = 0$), the viscous effects dominate over the convective term. Hence, when the fluid velocity is sufficiently small, the convection can be neglected. The momentum balance equation derived from the general Navier–Stokes system (3.1) then reads

$$\partial_t u - 2\nabla \cdot (\mu(x)\epsilon(u)) + (u \cdot \nabla)u + \nabla p = f, \qquad \text{in} \qquad (0,T] \times \Omega, \tag{3.1}$$

where the second term denotes the viscous contribution, while the third term represents convection. Under these assumptions, the problem reduces to the following linear system:

$$-\nabla \cdot (2\mu(x)\epsilon(u)) + \nabla p = f, \qquad \text{in} \qquad \Omega, \tag{3.2}$$

$$\nabla \cdot u = 0, \qquad \text{in} \qquad \Omega, \tag{3.3}$$

which is commonly referred to as the Stokes equations. In this study, this problem is subject to the non-slip boundary conditions

$$u = 0 \qquad \text{on} \qquad \Gamma, \tag{3.4}$$

where u is the fluid velocity field, p is the pressure, $\epsilon(u)$ is the symmetric deformation tensor given by $\epsilon(u) = \frac{1}{2}\left(\nabla u + (\nabla u)^T\right)$, f represents the external forces and $\mu(x)$ is the variable dynamic viscosity verified the inequality

$$0 < \mu_0 \ \le\ \mu(x)\ \le\ \mu_1 < \infty, \qquad \text{a.e.} \quad \text{in} \quad \Omega. \tag{3.5}$$

We introduce the following functional spaces:

$$V = \left\{v \mid v \in \left(H^1(\Omega)\right)^2, v = 0 \text{ on } \Gamma\right\} \tag{3.6}$$

$$Q = L^2_0(\Omega) = \left\{q \mid q \in L^2(\Omega), \int_\Omega q \, \mathrm{d}x = 0\right\}, \tag{3.7}$$

the Hilbert space Q is endowed with the classical inner product

$$(q,s) = \int_\Omega qs\, dx,$$

which induces the norm $\|q\|_Q = \|q\|_{L^2(\Omega)}$. For the velocity space V, two different inner products will be considered. To establish a μ-independent formulation, we equip V with the bilinear form

$$(\nabla v, \nabla w) = \int_\Omega \nabla v.\nabla w \, dx, \tag{3.8}$$

which induces the H_0^1-seminorm $|v|_{H_0^1(\Omega)} = \|\nabla v\|_0$.

Alternatively, we may consider the viscosity-dependent inner product

$$\big(\mu\epsilon(v), \epsilon(w)\big) = \int_\Omega \mu\epsilon(v).\epsilon(w) \, dx, \tag{3.9}$$

the associated norm is then defined as $\|v\|_\mu = \|\mu^{1/2}\epsilon(v)\|_0$.

Remark 3.1. Using the Poincaré inequality, it can be shown that both choices (3.8) and (3.9) indeed generate norms on V.

Lemma 3.1 (Korn inequality)**.** *A positive constant C_K, depending solely on the domain Ω, can be found such that*

$$\|\nabla v\|_0 \leq C_K \|\varepsilon(v)\|_0, \qquad \textit{for all} \qquad v \in V.$$

Proof. See [13] theorem 1.1-2. □

Lemma 3.2. *The equivalence of the two norms $\|.\|_\mu$ and $|.|_{H_0^1(\Omega)}$ is valid under the assumption that the viscosity μ is strictly positive*

Proof. Let $v \in V$, by definition of the deformation tensor and using the invariance of the Frobenius norm under transposition, we have

$$\|\varepsilon(v)\| = \left\| \frac{\nabla v + (\nabla v)^\top}{2} \right\| \leq \frac{1}{2}\big(\|\nabla v\| + \|(\nabla v)^\top\|\big) = \|\nabla v\|,$$

for any matrix norm $\|\cdot\|$, and in particular for the L^2-norm $\|\cdot\|_0$.

Now, let $\mu \in L^\infty(\Omega)$ satisfy (3.5), it follows that

$$\|v\|_\mu = \|\mu^{1/2}\varepsilon(v)\|_0 \ \leq \ \mu_{\max}^{1/2} \|\nabla v\|_0, \qquad \text{for all} \qquad v \in V.$$

On the other hand, since $v \in V$, Korn's inequality yields

$$\|\nabla v\|_0 \ \leq \ C_K \|\varepsilon(v)\|_0.$$

Moreover, from the bounds on μ, we deduce

$$\mu_{\min}^{1/2} \|\varepsilon(v)\|_0 \ \leq \ \|v\|_\mu \ \leq \ \mu_{\max}^{1/2} \|\varepsilon(v)\|_0.$$

Combining the two inequalities, we finally obtain

$$\|\nabla v\|_0 \ \leq \ C_K \mu_{\min}^{-1/2} \, \|v\|_\mu.$$

This establishes the equivalence between the norms $\|\nabla v\|_0$ and $\|v\|_\mu$, which completes the proof. □

To write a variational formulation for the problem (3.2) - (3.4), we multiply the two equations (3.2) - (3.3) by the test functions v and q, respectively. And integrating over Ω before applying the integral by parts, we seek to find $(u,p) \in V \times Q$ such that for all $(v,q) \in V \times Q$, the following equations are satisfied:

$$\int_\Omega 2\mu(x)\epsilon(u).\nabla v dx - \int_\Omega p\nabla \cdot v dx = \int_\Omega f \cdot v dx, \tag{3.10}$$

$$-\int_\Omega q\nabla \cdot u dx = 0, \tag{3.11}$$

from the equality,

$$\int_\Omega 2\mu(x)\epsilon(u).\nabla v dx = \int_\Omega 2\mu(x)\epsilon(u).\epsilon(v)dx, \tag{3.12}$$

an equivalent weak formulation becomes

$$\int_\Omega 2\mu(x)\epsilon(u).\epsilon(v)dx - \int_\Omega p\nabla \cdot v dx = \int_\Omega f \cdot v dx, \tag{3.13}$$

$$-\int_\Omega q\nabla \cdot u dx = 0. \tag{3.14}$$

Thanks to (3.5) and the uniform positivity and boundedness of $\mu(x)$, the classical theory of linear saddle point problems [4, 9] can be invoked to guarantee the existence and uniqueness of the solution to the problem.

4. Numerical scheme and algebraic form

The solution is obtained by solving the equations (3.2) - (3.4) discretely. To do this, we approximate the velocity u and pressure p fields by interpolation functions defined on each element of the mesh, as a way to utilize the isogeometric Galerkin method to the weak problem (3.10)-(3.11), the NURBS basis functions corresponding to the domain parametrization Ω applied to build spaces of discrete functions $V_h \subset V$ and $Q_h \subset Q$. The method belongs to the category of mixed finite elements since pressure and velocity are represented by different discrete spaces. For velocity, we use NURBS basis of degree $p+1$, and for pressure, we use NURBS basis of degree p. i.e in the parametric domain the Taylor-Hood velocity and pressure space are defined respectively by

$$V_h^{TH} := \text{span}\left\{e_k R_{i,j}^{p+1,p+1} \mid i = 1,\ldots,n; j = 1,\ldots,m; k = 1,2\right\}, \tag{4.1}$$

with e_k the canonical basis of $\mathbb{R}^2$,

$$Q_h^{TH} := \text{span}\left\{\mathrm{R}_{i,j}^{p,p} \mid i = 1,\ldots,n; j = 1,\ldots,m\right\}. \tag{4.2}$$

The NURBS-based Taylor–Hood finite element spaces defined over the physical domain are given by:

$$\begin{cases} \mathcal{V}_{\mathrm{h},0}^{\mathrm{TH}} := \text{span}\left\{\phi_{\mathbf{i}}^{k,\mathrm{TH}} := \varepsilon_k \mathrm{R}_{\mathbf{i}}^{p+1,p+1} \circ \mathbf{F}^{-1} \mid \mathbf{i} = 1,\ldots,\mathrm{n}_{\mathrm{V},k}^{\mathrm{TH}}; k = 1,2\right\}, \\ \mathcal{Q}_{\mathrm{h}}^{\mathrm{TH}} := \text{span}\left\{\rho_{\mathbf{i}}^{\mathrm{TH}} := \mathrm{R}_{\mathbf{i}}^{p,p} \circ \mathbf{F}^{-1} \mid \mathbf{i} = 1,\ldots,\mathrm{n}_{\mathcal{P}}^{\mathrm{TH}}\right\}. \end{cases} \tag{4.3}$$

Moreover, the pressure space $\mathcal{Q}_{\mathrm{h},0}^{\mathrm{TH}}$ is considered in the form:

$$\mathcal{Q}_{\mathrm{h},0}^{\mathrm{TH}} := \left\{ p \in \mathcal{Q}_{\mathrm{h}}^{\mathrm{TH}} \mid \int_{\Omega} p \mathrm{d}\Omega = 0 \right\}. \tag{4.4}$$

which allows us to define discrete spaces as follows

$$\mathcal{V}_h = V_{h,0}^{TH},$$
$$Q_h = Q_{h,0}^{TH},$$

the approximated problem becomes, find $(u_h, p_h) \in V_h \times Q_h$ such that

$$a(u_h, v_h) - b(p_h, v_h) = l(v_h), \quad \forall v_h \in \mathcal{V}_h, \tag{4.5}$$
$$-b(q_h, v_h) = 0, \quad \forall q_h \in \mathcal{Q}_h. \tag{4.6}$$

where $a : \mathcal{V}_h \times \mathcal{V}_h \to \mathbb{R}$ is the bilinear form defined by $a(u_h, v_h) = \int_\Omega \mu(x)\epsilon(u_h).\epsilon(v_h)d\Omega$, for all $(u_h, v_h) \in \mathcal{V}_h \times \mathcal{V}_h$, $b : \mathcal{Q}_h \times \mathcal{V}_h \to \mathbb{R}$ is the bilinear form defined by $b(q_h, v_h) = -\int_\Omega q_h \nabla \cdot v_h d\Omega$, for all $(q_h, v_h) \in \mathcal{Q}_h \times \mathcal{V}_h$, and $l : \mathcal{V}_h \to \mathbb{R}$ is the linear form defined by $l(v_h) = \int_\Omega f v_h d\Omega$, for all $v_h \in \mathcal{V}_h$.

The velocity is then approximated by

$$u_h = \sum_{i=1}^{N_u} \mathbf{R}_i^{p,q}(\xi)\mathbf{u}_i, \tag{4.7}$$

where $\mathbf{u}_i = (u_i, v_i)$ denotes the velocity control variables, and $\mathbf{R}i^{p,q} = (R_i^{p,q}, R_i^{p,q})$ represents the NURBS basis functions associated with the velocity. Similarly, the pressure are defined as linear combinations of NURBS basis functions, the pressure is then approximated by:

$$p_h = \sum_{i=1}^{N_p} R_i^{p,q}(\xi)p_i, \tag{4.8}$$

here, p_i are the pressure control variable. Since, from the discrete formulation (4.6), we obtain a large linear system as follows.

$$\begin{bmatrix} \mathcal{A} & \mathcal{B}^T \\ \mathcal{B} & 0 \end{bmatrix} \begin{bmatrix} \mathbf{u} \\ \mathbf{p} \end{bmatrix} = \begin{bmatrix} \mathbf{f} \\ 0 \end{bmatrix}, \tag{4.9}$$

which can be solved numerically to obtain the values of the unknowns $\mathbf{u}_i$ and $\mathbf{p}_i$. Finally, these values are used to reconstruct the velocity and pressure fields in the domain.

The matrix $\mathcal{A}$ of size $N_u \times N_u$ is symmetric positive definite (SPD) under the assumption that the viscosity coefficient satisfies $\mu(x) > 0$ almost everywhere in Ω. Indeed, the entries of $\mathcal{A}$ are defined by the viscous bilinear form

$$\mathcal{A}_{ij} = \int_\Omega \mu(x)\, \epsilon(\mathbf{R}_i^{p,q}) : \epsilon(\mathbf{R}_j^{p,q})\, d\Omega, \qquad i, j = 1, \ldots, N_u, \tag{4.10}$$

where $\epsilon(\mathbf{v}) = \frac{1}{2}(\nabla \mathbf{v} + \nabla \mathbf{v}^T)$ denotes the strain-rate tensor. The symmetry of $\mathcal{A}$ follows directly from the symmetry of the inner product, while its positive definiteness is guaranteed by

Korn's inequality together with the positivity of the viscosity coefficient. As a consequence, $\mathcal{A}$ is sparse, symmetric, and numerically well-conditioned compared with convection-dominated discretizations, provided that the viscosity is not extremely small.

The matrix $\mathcal{B}$, of size $N_u \times N_p$, represents the discrete divergence operator and is associated with the incompressibility constraint. Its entries are given by

$$\mathcal{B}_{ij} = -\int_\Omega (\nabla \cdot \mathbf{R}_i^{p,q})\, R_j^{p-1,q-1}\, d\Omega, \qquad i = 1, \ldots, N_u, \quad j = 1, \ldots, N_p. \tag{4.11}$$

The use of different approximation orders for velocity and pressure spaces is required to satisfy the inf-sup (Ladyzhenskaya–Babuška–Brezzi) stability condition, which ensures the numerical stability of the mixed formulation.

The right-hand side write as

$$\mathbf{f}_i = \int_\Omega f(x)\mathbf{R}_i^{p,q}(\boldsymbol{x})d\Omega, \qquad i = 1, ..., N_u. \tag{4.12}$$

The integrals appearing in equations (4.10)–(4.12) are numerically evaluated using Gauss quadrature with a 5 point rule on each direction in the forthcoming numerical experiments.

5. Numerical discussion

Numerical validation of the proposed method is presented in this section. As a first step, we consider a benchmark test with variable viscosity, denoted by $\mu_(x, y)$, on a curved domain. In Example 2, manufactured solutions are employed to demonstrate the convergence, efficiency, and accuracy of the proposed scheme in the case of linearly varying viscosity. Subsequently, the case of exponentially varying viscosity is addressed, along with a comparison to the classical finite element method. These detailed analyses allow us to assess the performance of our method in solving practical problems and to highlight its advantages over conventional approaches. All simulations are carried out using the MATLAB toolbox GeoPDEs [30].

5.1. A wall-driven semi-circular cavity

We conduct a simulation of semi-circular cavity flow driven by a wall. Our focus lies in examining the characteristics of the numerical method. The computational domain encompasses the geometric region of the flow.

$$\Omega = \left\{ \mathbf{x} = (x, y) \in R^2 \mid y < 0, x^2 + y^2 < 1/4 \right\}.$$

The computational domain Ω is considered figure (1), it is represented by NURBS functions see figure (1). In the first direction, we consider the knot $\Xi_1 = (0, 0, 0, 0.5, 0.5, 1, 1, 1)$, and in the second direction, we consider $\Xi_2 = (0, 0, 1, 1)$. Coordinates and weights for the points considered can be found in the appendix. We will compute the velocity field and pressure in this case using NURBS basis functions of degree $p = 3$ and the regularity $k = 2$ in each direction, with a 20×20 subdivision. Figure (2) depicts the pressure and velocity field, while figures (3) shows the behavior of the first and second velocity components. Along the straight segment of the boundary denoted by Γ_1, we prescribe a velocity condition of $u = (1, 0)$. For the curved portion Γ_2, we designate it as a slip boundary, as illustrated in Figure (1). The viscosity is defined as $\mu(x, y) = \mu_0(1 + (x^2 + y^2)/10)$, with $\mu_0 = 0.1$. Since the exact solutions for this problem are unknown, we consider both the augmented and standard formulations.

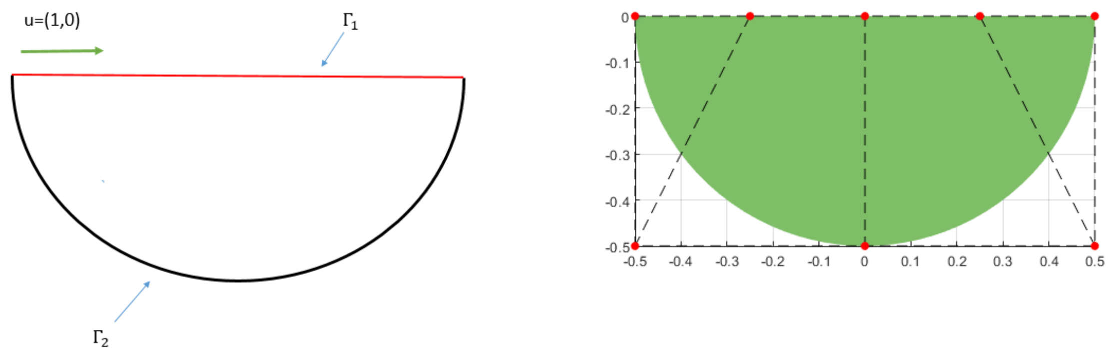

Figure 1. Wall-driven flow in a semi-circular cavity in the left, the semi-circular cavity with the control points in the right.

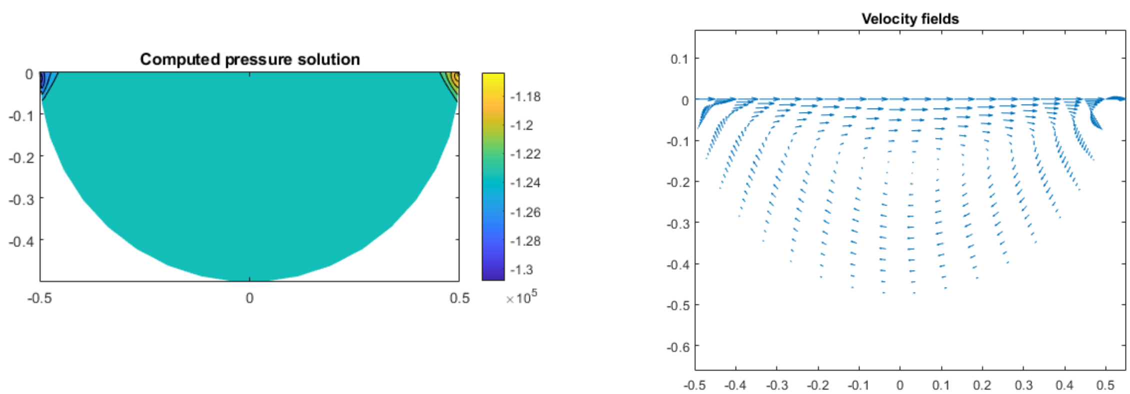

Figure 2. The pressure solution in the left, the vector field of velocity in the right.

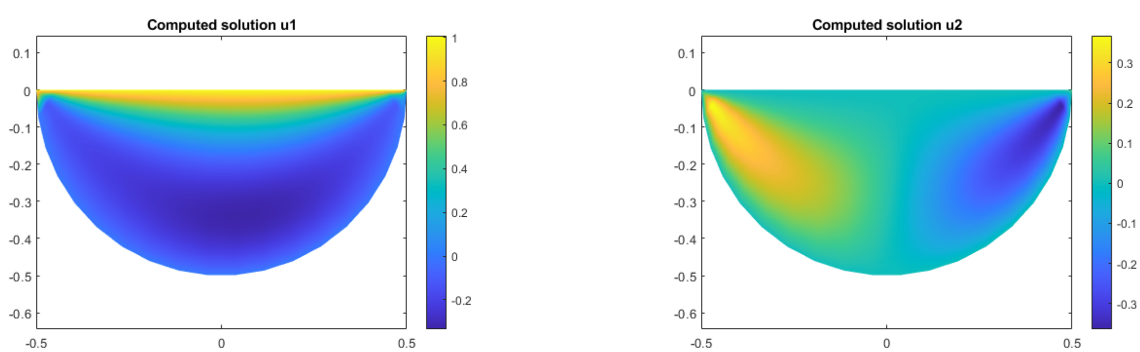

Figure 3. The first component of velocity in the left, the second component of velocity in the right.

5.2. A linear viscosity

The tested approach focuses on the Stokes problem with variable viscosity. A steady-state case is considered, where the exact solution is prescribed on the unit square $(0,1)^2$, following the idea presented in [21]. Homogeneous Dirichlet boundary conditions are applied, and the velocity field is constructed to be divergence-free by defining it as follows:

$$u = \begin{pmatrix} u_1 \\ u_2 \end{pmatrix} = \begin{pmatrix} \partial_y \psi \\ -\partial_x \psi \end{pmatrix}, \tag{5.1}$$

where ψ represents the stream function given by

$$\psi(x,y) = 100x^2(1-x)^2y^2(1-y)^2, \tag{5.2}$$

this yields

$$u(x,y) = 200 \begin{pmatrix} x^2(1-x)^2y(1-y)(1-2y) \\ -x(1-x)(1-2x)y^2(1-y)^2 \end{pmatrix}. \tag{5.3}$$

It is easy to verify that the solution 5.3 satisfies $\nabla \cdot u = \partial_x u_1 + \partial_y u_2 = 0$. The Stokes problem are supplemented with homogeneous Dirichlet boundary conditions, i.e.,

$$u = g = 0 \qquad \text{on} \qquad \Gamma. \tag{5.4}$$

To investigate the influence of viscosity on the numerical solution, we consider in this case the viscosity is defined by a linear expression reaches its minimal value $\mu_{\min}$ in $(0,0)$ and $\mu_{\max}$ in $(1,1)$, such described in the figure (4). Its expression it is expressed as follows

$$\mu_1(x,y) = \mu_{\min} + (\mu_{\max} - \mu_{\min})\, xy, \tag{5.5}$$

Figure 5 presents the error norms for the velocity and pressure. The velocity is evaluated using

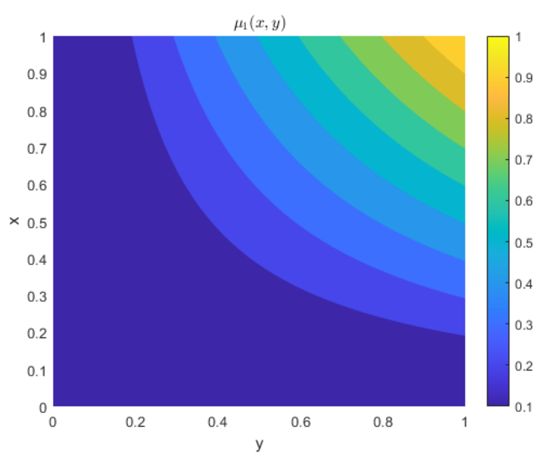

Figure 4. The linear viscosity.

both the L^2 and H^1-norm, while the pressure is assessed using the L^2-norm. In this test, we consider two cases to examine the convergence behavior of the proposed scheme. In the first case, the viscosity varies within a narrow range, with $\mu_{\min} = 0.1$ and $\mu_{\max} = 1$. In the second case, we consider a much larger variation, with $\mu_{\min} = 10^{-4}$ and $\mu_{\max} = 1$. The results obtained demonstrate the robustness and effectiveness of the developed scheme, even in the presence of a significant contrast between the minimum and maximum viscosity values. We notice that when we increase the gap between the minimum and maximum viscosity, the speed-dependent error becomes higher, while the pressure-dependent error remains the same.

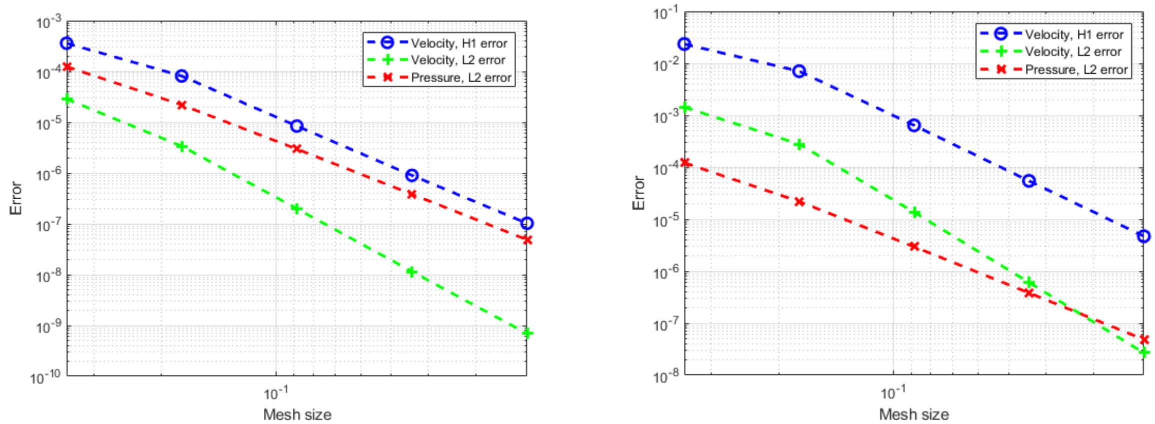

Figure 5. The error convergence for $\mu_{\min} = 0.1$ and $\mu_{\max} = 1$ left, and for $\mu_{\min} = 0.0001$ and $\mu_{\max} = 1$ right.

5.3. An exponential viscosity

The second case is characterized by a smoothly varying viscosity described by an exponential function, as illustrated in Figure 6. The viscosity distribution is defined by

$$\mu_2(x,y) = \mu_{\min} + (\mu_{\max} - \mu_{\min}) \exp\left(-10^{13}\left((x-0.5)^{10} + (y-0.5)^{10}\right)\right), \tag{5.6}$$

where $\mu_{\min}$ and $\mu_{\max}$ represent the minimum and maximum viscosity values, respectively. This formulation creates a highly localized region of high viscosity centered at the point $(0.5, 0.5)$, with a rapid decay away from the center. Such a profile is often used to model flows with sharp viscosity contrasts, which are common in heterogeneous materials or multiphase fluid systems.

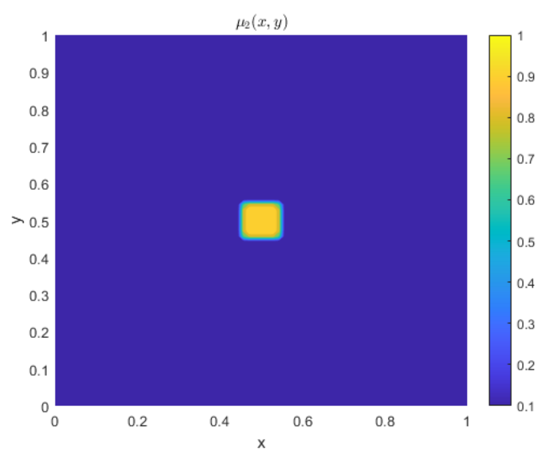

Figure 6. The exponential viscosity.

Figure 7 presents the convergence behavior of the proposed method for two different viscosity distributions. The left panel corresponds to a moderate viscosity contrast with $\mu_{\min} = 0.1$ and $\mu_{\max} = 1$, while the right panel illustrates a highly heterogeneous case where $\mu_{\min} = 10^{-4}$ and $\mu_{\max} = 1$. In both cases, the method demonstrates optimal convergence rates for the velocity and pressure errors. More specifically, the H^1 and L^2 norms of the velocity exhibit the expected theoretical rates, with a clear reduction in the error as the mesh is refined. The pressure L^2

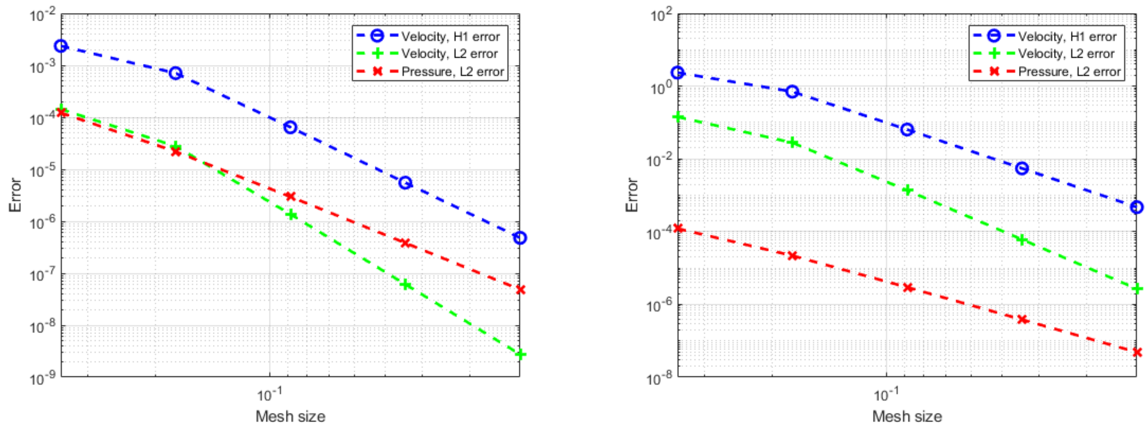

Figure 7. The error convergence for $\mu_{\min} = 0.1$ and $\mu_{\max} = 1$ in the left, $\mu_{\min} = 0.0001$ and $\mu_{\max} = 1$ in the right.

error also decreases consistently, confirming the stability of the mixed formulation. It is worth noting that, in the highly heterogeneous case, the convergence remains robust despite the strong viscosity variations, which highlights the capability of the proposed discretization to handle sharp gradients and localized features in the viscosity field.

5.4. Vortex flow: Comparaison test

In this subsection, we present a numerical comparison between the ST-EG [17] and IGA Taylor–Hood methods based on the vortex flow benchmark problem defined on the computational domain $\Omega = (0,1) \times (0,1)$. The considered test case is constructed using an analytical exact solution for both the velocity and pressure fields of (3.2)-(3.3),

$$\mathbf{u} = \begin{pmatrix} 10x^2(x-1)^2 y(y-1)(2y-1) \\ -10x(x-1)(2x-1)y^2(y-1)^2 \end{pmatrix}, \qquad p = 10(2x-1)(2y-1).$$

The corresponding body force and Dirichlet boundary conditions are derived from the governing equations using the exact solution. To evaluate the performance of both methods, a mesh refinement study is conducted by progressively decreasing the mesh size h while keeping the viscosity fixed at $\mu = 10^{-6}$.

Table 1. Mesh refinement study for ST-EG [17] and IGA Taylor-Hood.

	ST-EG				IGA Tayloor Hood			
h	$\|u-u_h\|$	Rate	$\|p-p_h\|_{L^2}$	Rate	$\|u-u_h\|$	Rate	$\|p-p_h\|_{L^2}$	Rate
1/4	1.959e+5	–	1.166e+0	–	7.41486e-03	–	1.63671e-09	–
1/8	7.140e+4	1.46	5.180e-1	1.17	1.07806e-03	2.78	3.85710e-11	5.41
1/16	2.468e+4	1.53	2.483e-1	1.06	1.44820e-04	2.90	8.49539e-13	5.50
1/32	8.552e+3	1.53	1.223e-1	1.02	1.88048e-05	2.95	1.79681e-14	5.56
1/64	2.987e+3	1.52	6.078e-2	1.01	2.39920e-06	2.97	4.42254e-15	5.59

Based on the exact solution presented above, we analyze the numerical accuracy of the two considered methods. The results in the table 1 clearly show that both the velocity and pressure errors decrease as the mesh size h is refined, which confirms the numerical convergence of both methods.

The observed convergence rates for the velocity errors are higher than first order for both approaches. More precisely, the ST-EG method exhibits a convergence rate of approximately 1.5, which is consistent with the theoretical error estimates.

However, the IGA Taylor–Hood method yields significantly smaller velocity errors compared to the ST-EG method. In particular, the velocity errors obtained using the IGA Taylor–Hood approach are several orders of magnitude smaller, indicating a higher numerical accuracy for the velocity field. Moreover, this method achieves higher convergence rates, close to order 3, which reflects the high approximation capability of IGA basis functions in representing smooth solutions.

Regarding pressure errors, both methods produce very small L^2-norm errors. Nevertheless, the IGA Taylor–Hood method again provides smaller pressure errors, reaching values close to machine precision, which demonstrates excellent numerical stability for this test case.

Overall, these numerical results indicate that the IGA Taylor–Hood method provides superior accuracy compared to the ST-EG method for this benchmark problem, while also confirming the validity of the theoretical convergence estimates.

6. Conclusion

In this paper, we presented a solution for Stokes problems with variable viscosity using mixed finite elements based on NURBS functions. Two numerical tests are provided: The first is a simulation of a semi-circular cavity, and the second is a numerical study of the convergence of our proposed method, considering two types of viscosity.

Future plans include the numerical analysis of coupled problems, specifically those where viscosity exhibits a dependency on the solution in a nonlinear manner.

Acknowledgements

The authors would like to express their sincere gratitude to the anonymous reviewers for their valuable comments, constructive suggestions, and careful reading of the manuscript. Their insightful remarks have significantly contributed to improving the quality, clarity, and presentation of this work.

References

[1] C. Aricò, R. Helmig and I. Yotov, *Mixed finite element projection methods for the unsteady stokes equations*, Computer Methods in Applied Mechanics and Engineering, 2025, 435, 117616.

[2] D. N. Arnold, F. Brezzi and M. Fortin, *A stable finite element for the stokes equations*, Calcolo, 1984, 21(4), 337–344.

[3] R. M. Aronson and J. A. Evans, *Divergence-conforming isogeometric collocation methods for the incompressible navier–stokes equations*, Computer Methods in Applied Mechanics and Engineering, 2023, 410, 115990.

[4] I. Babuška, *The finite element method with lagrangian multipliers*, Numerische Mathematik, 1973, 20(3), 179–192.

[5] C. De Boor and C. De Boor, *A Practical Guide to Splines*, 27, Springer-Verlag New York, 1978.

[6] M. Bosy, M. Montardini, G. Sangalli and M. Tani, *A domain decomposition method for isogeometric multi-patch problems with inexact local solvers*, Computers & Mathematics with Applications, 2020, 80(11), 2604–2621.

[7] A. Bressan, *Isogeometric regular discretization for the stokes problem*, IMA Journal of Numerical Analysis, 2011, 31(4), 1334–1356.

[8] A. Bressan and G. Sangalli, *Isogeometric discretizations of the stokes problem: Stability analysis by the macroelement technique*, IMA Journal of Numerical Analysis, 2013, 33(2), 629–651.

[9] F. Brezzi, *On the existence, uniqueness and approximation of saddle-point problems arising from lagrangian multipliers*, Publications des Séminaires de Mathématiques et Informatique de Rennes, 1974, (S4), 1–26.

[10] A. Buffa, C. De Falco and G. Sangalli, *Isogeometric analysis: Stable elements for the 2d stokes equation*, International Journal for Numerical Methods in Fluids, 2011, 65(11–12), 1407–1422.

[11] C. Burstedde, O. Ghattas, G. Stadler, et al., *Parallel scalable adjoint-based adaptive solution of variable-viscosity stokes flow problems*, Computer Methods in Applied Mechanics and Engineering, 2009, 198(21–26), 1691–1700.

[12] A. Cangiani, V. Gyrya and G. Manzini, *The non-conforming virtual element method for the stokes equations*, SIAM Journal on Numerical Analysis, 2016, 54(6), 3411–3435.

[13] P. G. Ciarlet, *Mathematical Elasticity. Volume II: Theory of Plates, Volume 27 of* Studies in Mathematics and its Applications, 1997.

[14] J. A. Cottrell, T. J. Hughes and Y. Bazilevs, *Isogeometric Analysis: Toward Integration of CAD and FEA*, John Wiley & Sons, 2009.

[15] J. A. Evans and T. J. Hughes, *Isogeometric divergence-conforming b-splines for the darcy–stokes–brinkman equations*, Mathematical Models and Methods in Applied Sciences, 2013, 23(04), 671–741.

[16] T. Hoang, C. V. Verhoosel, F. Auricchio, et al., *Mixed isogeometric finite cell methods for the stokes problem*, Computer Methods in Applied Mechanics and Engineering, 2017, 316, 400–423.

[17] X. Hu, S. Lee, L. Mu and S.-Y. Yi, *Pressure-robust enriched galerkin methods for the stokes equations*, Journal of Computational and Applied Mathematics, 2024, 436, 115449.

[18] T. J. Hughes, J. A. Cottrell and Y. Bazilevs, *Isogeometric analysis: Cad, finite elements, nurbs, exact geometry and mesh refinement*, Computer Methods in Applied Mechanics and Engineering, 2005, 194(39–41), 4135–4195.

[19] E. Jamelot, *Stability estimates for solving stokes problem with nonconforming finite elements*, Comptes Rendus. Mathématique, 2025, 363(G2), 115–137.

[20] V. John, K. Kaiser and J. Novo, *Finite element methods for the incompressible stokes equations with variable viscosity*, ZAMM-Journal of Applied Mathematics and Mechanics/Zeitschrift für Angewandte Mathematik und Mechanik, 2016, 96(2), 205–216.

[21] K. Kaiser, *Finite element methods for the incompressible stokes equations with non-constant viscosity*, Order, 2014, 1, 51.

[22] M. Kronbichler, T. Heister and W. Bangerth, *High accuracy mantle convection simulation through modern numerical methods*, Geophysical Journal International, 2012, 191(1), 12–29.

[23] L. E. Ouadefli, O. E. Moutea, A. E. Akkad, et al., *Mixed isogeometric analysis of the brinkman equation*, Mathematics, 2023, 11(12), 2750.

[24] P. R. Patil and G. Vaidyanathan, *Effect of variable viscosity on thermohaline convection in a porous medium*, Journal of Hydrology, 1982, 57(1–2), 147–161.

[25] L. Piegl and W. Tiller, *The NURBS Book*, Springer Science & Business Media, 2012.

[26] A. H. Poza and R. Rebolledo, *Equal-order finite element method for the stokes equations with variable viscosity*, Applied Mathematics Letters, 2024, 149, 108930.

[27] D. F. Rogers, *An Introduction to NURBS: With Historical Perspective*, Morgan Kaufmann, 2001.

[28] J. Rudi, G. Stadler and O. Ghattas, *Weighted bfbt preconditioner for stokes flow problems with highly heterogeneous viscosity*, SIAM Journal on Scientific Computing, 2017, 39(5), S272–S297.

[29] F. X. Trias, A. Gorobets and A. Oliva, *A simple approach to discretize the viscous term with spatially varying (eddy-) viscosity*, Journal of Computational Physics, 2013, 253, 405–417.

[30] R. Vázquez, *A new design for the implementation of isogeometric analysis in octave and matlab: Geopdes 3.0*, Computers & Mathematics with Applications, 2016, 72(3), 523–554.

[31] L. B. Da Veiga, A. Buffa, G. Sangalli and R. Vázquez, *Mathematical analysis of variational isogeometric methods*, Acta Numerica, 2014, 23, 157–287.

[32] J. Zhao, B. Zhang, S. Mao and S. Chen, *The divergence-free nonconforming virtual element for the stokes problem*, SIAM Journal on Numerical Analysis, 2019, 57(6), 2730–2759.

Received September 2025; Accepted March 2026; Available online June 2026.